Basic Kinematic Electron Diffraction

In 1986, E. Ruska was awarded the Nobel Physics Prize for his pioneering work of building the world's first transmission electron microscope (TEM) in the late 1920s. The TEM was originally based on the physical principle that charged particles can be focused by magnetic lenses. The strong interaction of incident electrons with electrons and nuclei in crystals makes it feasible to analyze structures of solids based on electron micrographs. The rapid development of TEM techniques in the last 30 years has made it possible to image crystal structures at atomic resolution. Thus TEM has become one of the key research tools in characterizing condensed matter.

Since electrons are charged particles, their interaction with a solid is rather strong in comparison to either X-ray or neutrons, so that multiple scattering effects are always present in electron diffraction. This means that electron diffraction has to be described by dynamic scattering theory especially when quantitative structural analysis is necessary. Dynamical theories, as shown in Chapters 2–5, are usually based on some fundamental quantities, defined in kinematic scattering theory, for describing the basic characteristics of electron diffraction. Chapter 1 outlines some basic concepts of kinematic electron-scattering theory and introduces a few mathematical operations used in this book. A systematic kinematic treatment of electron diffraction for perfect and imperfect crystal has been given by Cowley (1981).

1.1. WAVE PROPERTIES OF ELECTRONS

Although TEM was based on the optical behavior of charged particles, the electron diffraction is due purely to the wave property of particles. The wavelength λ of an electron is related to its momentum p by the de Broglie relation,

$$\lambda = \frac{h}{p} \tag{1.1}$$

In TEM, if the electron is accelerated to a kinetic energy of eU_0 , relativity theory indicates that the momentum p satisfies

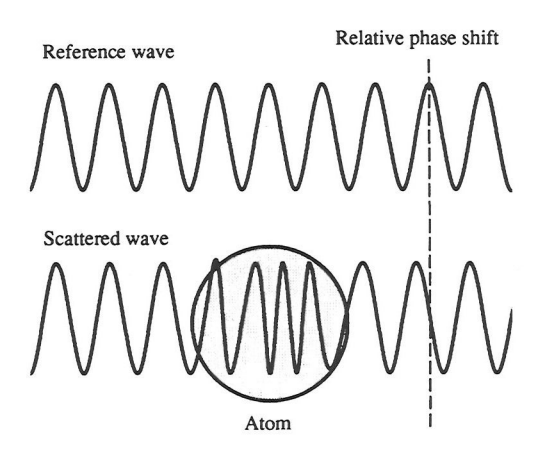


Figure 1.1. A schematic diagram showing the phase perturbation effect of an incident high-energy electron wave by the scattering of a single atom. The relative phase shift of the scattered wave with respect to the unscattered wave (or reference wave) is indicated by a dashed line.

$$eU_0 = (m_0^2 c_0^4 + p^2 c_0^2)^{1/2} - m_0 c_0^2$$
 (1.2)

where $m_0c_0^2$ is the rest energy of an electron. Substituting the solution of p from Eq. (1.2) into Eq. (1.1), the electron wavelength is

$$\lambda = \frac{h}{\{[2m_0eU_0[1 + eU_0/2m_0c_0^2]\}^{1/2}}$$
(1.3)

Substituting the numerical values of the fundamental physical constants, yields

$$\lambda = \frac{1.226}{\left[U_0(1 + 0.9788 \times 10^{-6} U_0)\right]^{1/2}} \,\text{nm}$$
 (1.4)

where U_0 is measured in volts. For 100 kV electrons, $\lambda = 0.0037$ nm. For such a small wavelength, a significant phase shift can be created if there is a small change in the scattering potential. A slight modification in crystal potential due to structural evolution can dramatically affect the scattering behavior of the electron. Since the atom size is less than 0.05 nm, a large phase variation can be created after the electron interacts with the atom (Fig. 1.1). This is approximately the origin of atomic resolution phase contrast lattice images of thin crystals using transmitted high-energy electrons (see many articles in Buseck et al., 1988). Wavelengths for electrons accelerated to different energies are listed in Appendix A.

1.2. PLANE WAVE

In electron imaging and diffraction, an incident electron is expressed as a plane wave. In free space and a nonrelativistic case, the propagation of an electron satisfies the time-dependent Schrödinger equation

$$-\frac{\hbar^2}{2m_0}\nabla^2 \Psi = -i\hbar \frac{\partial \Psi}{\partial t}$$
 (1.5)

For an infinity large free space, the plane wave solution of this equation is

$$\Psi = \exp(2\pi i \mathbf{K}_0 \cdot \mathbf{r} + i\omega t) \tag{1.6}$$

where

$$\hbar\omega = \frac{h^2 K_0^2}{2m_0} = E$$

is the electron kinetic energy and $K_0 = 1/\lambda$ is the electron wave number. The scattering of the electron by a crystal is treated as the scattering of the plane wave by the potential field of the solid. Since electron diffraction is usually a time-independent scattering process, the time-dependent factor $\exp(i\omega t)$ is dropped in the following discussion. In this book, $\exp(2\pi i \mathbf{K}_0 \cdot \mathbf{r})$ is taken as a plane wave with wave vector \mathbf{K}_0 . The sign of the phase factor $(2\pi i)$ is kept consistent in the entire book.

1.3. SINGLE-ATOM SCATTERING

The easiest case in electron diffraction is scattering by a single atom. In this case, the electron is scattered due to its interaction with the electrostatic potential of the atom. In high-energy electrons, if the scattering potential $V(\mathbf{r})$ is weak, the amplitude of an incident plane wave $\exp(2\pi i \mathbf{K}_0 \cdot \mathbf{r})$ to be scattered to an exit plane wave of wave vector \mathbf{K} is calculated by the first Born approximation,

$$f(\mathbf{u}) = -\frac{m_0}{2\pi\hbar^2} \int d\mathbf{r} \exp(-2\pi i \mathbf{u} \cdot \mathbf{r}) \ V(\mathbf{r})$$
 (1.7)

where $\hbar \mathbf{u} = \hbar (\mathbf{K} - \mathbf{K}_0)$ is the momentum transfer of the incident electron. The Born approximation assumes single scattering; that is, the electron is scattered only once. This assumption is the basis of kinematic scattering theory. If the atomic potential is spherical symmetric, i.e., $V(\mathbf{r}) = V(r)$, Eq. (1.7) becomes

$$f(\theta) = -\frac{2m_0}{\hbar^2} \int_{0}^{\infty} dr \frac{\sin 2\pi u r}{2\pi u r} V(r) r^2$$
 (1.8)

where 2θ is the scattering angle shown in Fig. 1.2 and $\mathbf{u} = \mathbf{K} - \mathbf{K}_0$ with $u = 2K \sin \theta$. The scattering power of the atom is determined by the Fourier transform (**FT**) of its electrostatic potential; thus the electron-scattering factor of the atom is defined as

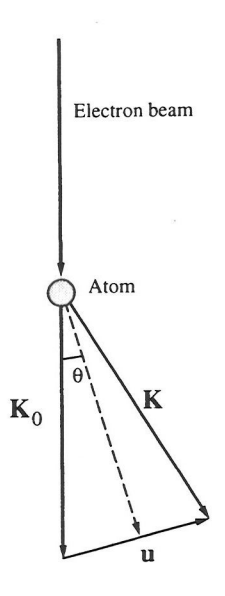


Figure 1.2. Kinematic scattering of an incident plan wave by a single atom under the Born approximation. The change of electron momentum if $\hbar u$.

$$f^{e}(\mathbf{u}) = \int d\mathbf{r} \exp(-4\pi i \mathbf{s} \cdot \mathbf{r}) \ V(\mathbf{r})$$
 (1.9)

where the scattering vector is defined as $s = \sin \theta / \lambda$, or s = u/2, with u a reciprocal space vector (see Section 1.6). The electron-scattering factor is usually given as a function of s. For the convenience of mathematical expressions in this book, we use u as the variable of $f^e(u)$. The electron-scattering factor defined in Eq. (1.9) is a quantity that characterizes the scattering power of an atom, and it is independent of the accelerating voltage.

1.4. MOTT FORMULA

The electron-scattering factor is usually difficult to measure experimentally because electron scattering in crystals is a dynamic scattering process. Thus, the scattering of an electron is determined by a solution of the Schrödinger equation. The X-ray diffraction, on the other hand, is usually treated kinematically for thin crystals, and quantitative data analysis is possible using kinematic scattering theory. This is why X-ray diffraction is one of the most accurate methods for structural determination. Since the interaction of X rays (or electromagnetic waves) with a crystal is determined by the charge distribution in the crystal, it is possible to correlate the potential function of an atom with its charge distribution using

Maxwell's equations. For an atom of atomic number Z_0 , the electrostatic potential function and electron charge density function are related by the Poisson equation

$$\nabla^2 V_{\kappa}(\mathbf{r}) = -\frac{e}{\varepsilon_0} [Z_0 \delta(\mathbf{r}) - \rho_{\kappa}(\mathbf{r})]$$
 (1.10)

where $\delta(\mathbf{r})$ is the Dirac delta function indicating the position of the nucleus. Taking a Fourier transform of Eq. (1.10), then using Eq. (1.9) and the X-ray scattering factor defined by

$$f_{\kappa}^{x}(\mathbf{s}) = \int d\mathbf{r} \exp(-4\pi i \mathbf{s} \cdot \mathbf{r}) \, \rho_{\kappa}(\mathbf{r}) \tag{1.11}$$

we have

$$(4\pi is)^2 f_{\kappa}^e(\mathbf{u}) = -\frac{e}{\varepsilon_0} [Z_0 - f_{\kappa}^x(\mathbf{s})]$$

or

$$f_{\kappa}^{e}(\mathbf{u}) = \frac{e}{16\pi^{2}\epsilon_{0}} \frac{[Z_{0} - f_{\kappa}^{x}(\mathbf{s})]}{\mathbf{s}^{2}}$$
(1.12)

This is the well-known Mott formula, from which the electron-scattering factor can be directly calculated using the experimentally measured X-ray scattering factor. For general purpose, f^x can be written in analytic form in terms of the Gaussian functions (Doyle and Turner, 1968).

$$f^{x}(s) = \sum_{i=1}^{4} a_{i} \exp(-b_{i}s^{2}) + c_{i}$$
 (1.13)

where the fitting parameters a_i and b_i have been determined for most of the elements in neutral and ionized states. For high-energy electrons, the correction introduced by the exchange effect of valence electrons on the atomic-scattering factor is negligible, so that the scattering factor defined in Eq. (1.13) is independent of the incident energy of the electrons. This approximation may not hold if the energy of the incident electron is lower than a few keV (Qian et al., 1993). For atoms with spherical symmetry, the atomic-scattering factor is a real function. The atomic-scattering factor could be a complex function if the atomic potential were not absolutely spherically symmetric due to charge redistribution or exchange resulted from solid bonding.

The asymptotic behavior of the scattering factors for large and small values of s must be considered (Peng and Cowley, 1988). The electron-scattering factor must converge to the Rutherford-scattering form at high angles. The convergence of f^e at s=0 requires that $f^x(0)=Z_0$ according to the Mott formula or equivalently

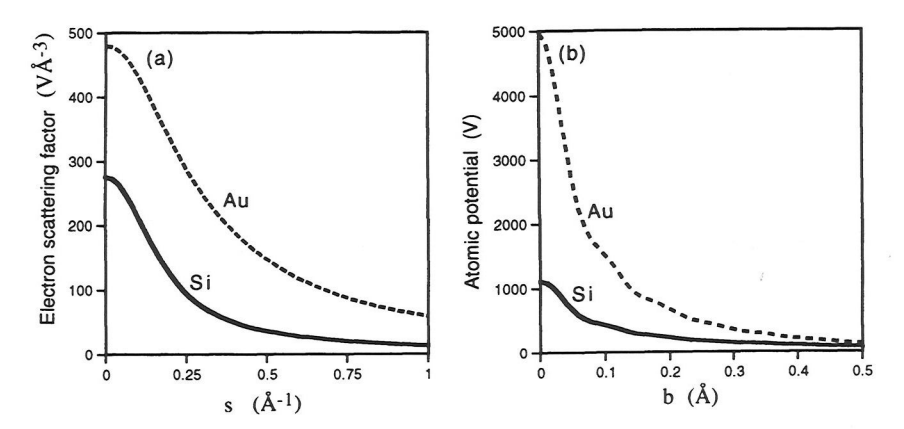


Figure 1.3. A comparison of (a) electron-scattering factors and (b) atomic potentials of gold and silicon atoms, showing the increase in atom-scattering power with an increased atomic number, where $s = \frac{\sin \theta}{1}$ and $b = (x^2 + y^2)^{\frac{1}{2}}$.

$$f^{x}(0) = Z_0 = \sum_{i=1}^{4} a_i + C_i$$

The empirical analytic expression given by Eq. (1.13) tends to deviate from the measured scattering factor when $s > 2 \text{ Å}^{-1}$. In this case, the expression proposed by Weickenmeier and Kohl (1991) gives better fit especially for $1.5 < s < 3 \text{ Å}^{-1}$

$$f^{e}(\mathbf{s}) = s^{-2} \sum_{i=1}^{6} A_{i} [1 - \exp(-B_{i}s^{2})]$$

where A_i and B_i are fitting parameters.

Figure 1.3a compares electron-scattering factors of silicon and gold, and Fig. 1.3b shows the corresponding atomic potentials. It is apparent that the scattering power of Au is much stronger than that of Si. The height of the potential peak is a direct measure of the high-angle scattering power of the atom. The full width of the half-maximum of the potential peak is about 0.2 Å.

1.5. KINEMATIC ELECTRON DIFFRACTION IN THIN CRYSTALS

If a crystal is very thin and the crystal potential is weak, then electron scattering can be treated kinematically; i.e., the electron is scattered only once, and there are no multiple-scattering effects. We first consider a three-dimensional periodic

crystal of finite size. The shape of this crystal is described by the shape function $S_p(\mathbf{r})$, as illustrated in Fig. 1.4. Under the rigid-body approximation, the potential distribution in real space \mathbf{r} is written as a superposition of the atomic potentials

$$V(\mathbf{r}) = \left\{ \sum_{n} \sum_{\alpha} V_{\alpha}(\mathbf{r} - \mathbf{R}_{n} - \mathbf{r}_{\alpha}) \right\} S_{p}(\mathbf{r})$$
(1.14)

where n is summed over all unit cells filling the entire space (i.e., $-\infty < n < \infty$) and α is summed over all atoms within a unit cell. The kinematic-scattering amplitude of the crystal is a Fourier transform of Eq. (1.14) according to the Born approximation,

$$V(\mathbf{u}) = \mathbf{FT}[V(\mathbf{r})] = \left\{ \sum_{n} \sum_{\alpha} \int d\mathbf{r} \, V_{\alpha}(\mathbf{r} - \mathbf{R}_{n} - \mathbf{r}_{\alpha}) \, \exp(-2\pi i \mathbf{u} \cdot \mathbf{r}) \right\} \otimes S_{p}(\mathbf{u})$$

$$= \left\{ \sum_{n} \exp(-2\pi i \mathbf{u} \cdot \mathbf{R}_{n}) \sum_{\alpha} \int d\mathbf{r} \, V_{\alpha}(\mathbf{r}) \, \exp(-2\pi i \mathbf{u} \cdot \mathbf{r}) \, \exp(-2\pi i \mathbf{u} \cdot \mathbf{r}_{\alpha}) \right\} \otimes S_{p}(\mathbf{u})$$

$$= \left\{ \sum_{g} \delta(\mathbf{u} - \mathbf{g}) \sum_{\alpha} V_{\alpha}(\mathbf{u}) \, \exp(-2\pi i \mathbf{u} \cdot \mathbf{r}_{\alpha}) \right\} \otimes S_{p}(\mathbf{u})$$

$$= \left\{ \sum_{g} \delta(\mathbf{u} - \mathbf{g}) \sum_{\alpha} V_{\alpha}(\mathbf{g}) \, \exp(-2\pi i \mathbf{g} \cdot \mathbf{r}_{\alpha}) \right\} \otimes S_{p}(\mathbf{u})$$

$$= \left\{ \sum_{g} \delta(\mathbf{u} - \mathbf{g}) \, V_{g} \right\} \otimes S_{p}(\mathbf{u})$$

$$(1.15)$$

where ⊗ indicates a convolution calculation (see Section 1.8) and the Fourier coefficient of the crystal potential is defined as

$$V_{g} = \frac{1}{\Omega} \sum_{\alpha} f_{\alpha}(g) < \exp[2\pi i \mathbf{g} \cdot (\mathbf{r}_{\alpha} + \mathbf{u}_{\alpha})] > = \sum_{\alpha} V_{\alpha}(\mathbf{g}) \exp(-2\pi i \mathbf{g} \cdot \mathbf{r}_{\alpha})$$
 (1.16a)

the scattering power of the α th atom in the unit cell is

$$V_{\alpha}(\mathbf{g}) = \frac{1}{\Omega} f_{\alpha}^{e}(\mathbf{g}) \exp\left[-W_{\alpha}(g)\right]$$
 (1.16b)

where the time average <> is introduced to take into account the thermal vibration effect of the atom near its equilibrium position; \mathbf{u}_{α} is the time-dependent displacement of the atom; and $\exp\left[-W_{\alpha}(g)\right] = \exp\left(-2\pi^2 < A_{\alpha}^2 > g^2\right)$ is the Debye-Waller (DW) factor, which is included in all elastic-scattering calculations to characterize weakening of the scattering power of an atom due to its thermal vibration. In deriving Eq. (1.15), an identity

$$\sum_{n} \exp(-2\pi i \mathbf{u} \cdot \mathbf{R}_{n}) = \sum_{g} \delta(\mathbf{u} - \mathbf{g})$$
 (1.17)

was used, where g is defined as a reciprocal lattice vector satisfying

$$\mathbf{g} \cdot \mathbf{R}_n = \mathbf{g} \cdot (n_1 \mathbf{a} + n_2 \mathbf{b} + n_3 \mathbf{c}) = \text{integer}$$
 (1.18)

 n_1 , n_2 , and n_3 are integers; \mathbf{a} , \mathbf{b} , and \mathbf{c} are the base vectors of the unit cell. The Dirac delta function $\delta(\mathbf{u} - \mathbf{g})$ allows only reflections that satisfy the Bragg's law in reciprocal space \mathbf{u} . The intensity of each Bragg reflection is scaled by $|V_g|^2$, conditions under which $V_g = 0$ for some \mathbf{g} s give extinction rules for forbidden reflections under the kinematic-scattering approximation. The forbidden reflections, however, may appear in the diffraction pattern if the multiple-scattering effect is dominant (Gjønnes and Moodie, 1965). The sharp Bragg reflections are broadened due to the convolution of the crystal shape factor S_p . Here we have introduced the concept of reciprocal space, Bragg's law, the convolution operation, and the Dirac delta function. Detailed discussions of these are given in the next few sections.

It is very important to point out that Eq. (1.17) is a key equation for converting a summation over unit cells in real space into a summation of reciprocal lattice vectors. This equation is frequently used in the following mathematical operations.

To illustrate the nature of the terms appearing in Eq. (1.15), Fig. 1.5 shows two electron diffraction patterns of a thin MgO crystal oriented along [100] and [110]. Each Bragg reflection is positioned at a reciprocal lattice point ${\bf g}$, and the intensity of this reflection is scaled (in kinematic scattering theory) according to $|V_g|^2$. The intensity at non-Bragg reflection positions is simply zero. Diffraction spots that are absent in diffraction patterns are those where the structure factors vanish. The (001) and (011) reflections of MgO are such examples.

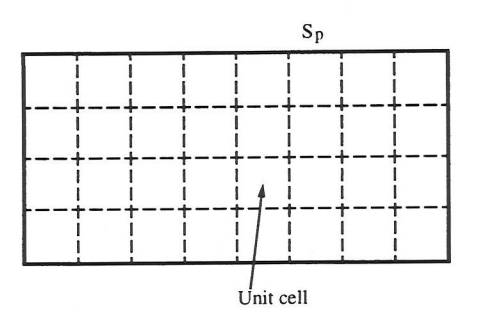


Figure 1.4. A finite-size periodically structured crystal defined by a shape function S_p . The blocks enclosed by dashed lines represent the distribution of crystal unit cells.

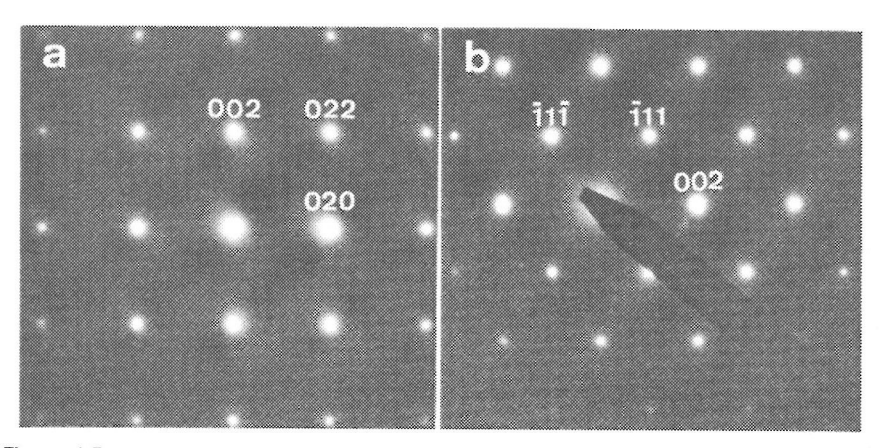


Figure 1.5. Transmission electron diffraction patterns recorded at 100 keV from an MgO crystal oriented along (a) [100] and (b) [110] directions. The central transmitted (000) beam in (b) was blocked by a beam stop.

1.6. RECIPROCAL SPACE

As shown in Eq. (1.18), reciprocal space is defined by a vector $\mathbf{g} = \ell \mathbf{a}^* + m\mathbf{b}^* + n\mathbf{c}^*$, where (ℓ, m, n) are the Miller indices of \mathbf{g} and satisfy

$$(\mathscr{C}\mathbf{a}^* + m\mathbf{b}^* + n\mathbf{c}^*) \cdot (n_1\mathbf{a} + n_2\mathbf{b} + n_3\mathbf{c}) = \text{integer}$$
 (1.19)

This equation can be satisfied by choosing

$$\mathbf{a}^* = \frac{\mathbf{b} \times \mathbf{c}}{\Omega} \quad \mathbf{b}^* = \frac{\mathbf{c} \times \mathbf{a}}{\Omega} \quad \mathbf{c}^* = \frac{\mathbf{a} \times \mathbf{b}}{\Omega}$$
 (1.20)

where $\Omega = (\mathbf{a} \times \mathbf{b}) \cdot \mathbf{c}$ is the volume of the unit cell. It can easily be proved

$$\mathbf{a}^* \cdot \mathbf{b} = \mathbf{a}^* \cdot \mathbf{c} = \mathbf{b}^* \cdot \mathbf{a} = \dots = 0 \tag{1.21a}$$

and

$$\mathbf{a}^* \cdot \mathbf{a} = \mathbf{b}^* \cdot \mathbf{b} = \mathbf{c}^* \cdot \mathbf{c} = 1 \tag{1.21b}$$

The space defined by base vectors $(\mathbf{a}^*, \mathbf{b}^*, \mathbf{c}^*)$ is called reciprocal space (or momentum space). A point in reciprocal space specifies the electrons traveling in the same direction in real space. A high-resolution lattice image in real space is the interference result of electron beams located at different points in reciprocal space. Therefore the angular distribution of scattered electrons is more conveniently described in reciprocal space. Figure 1.6 shows a crystal unit cell and corresponding reciprocal lattice vectors.

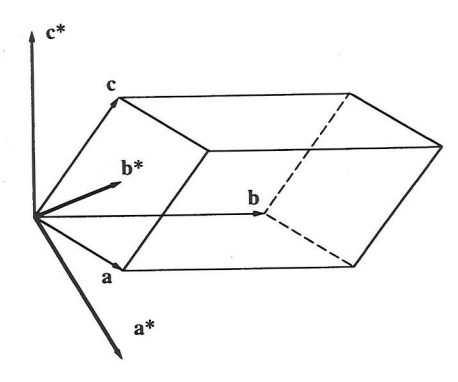


Figure 1.6. Relationships between the lattice vectors of a crystal unit cell and the corresponding reciprocal lattice vectors.

1.7. BRAGG'S LAW

As shown in Eq. (1.15), the diffraction of a perfect crystal forms a set of sharp peaks distributed at the reciprocal lattice sites defined by $\mathbf{g} = \ell \mathbf{a}^* + m\mathbf{b}^* + n\mathbf{c}^*$. A strong reflection peak is generated if the change in electron wave vector $\mathbf{u} = \mathbf{K} - \mathbf{K}_0$ equals the reciprocal space vector \mathbf{g} ,

$$\mathbf{u} = \mathbf{\ell} \mathbf{a}^* + m\mathbf{b}^* + n\mathbf{c}^* \tag{1.22}$$

This is exactly the result of conservation of momentum in elastic electron scattering. The meaning of Eq. (1.22) can be clearly stated using the Ewald sphere construction

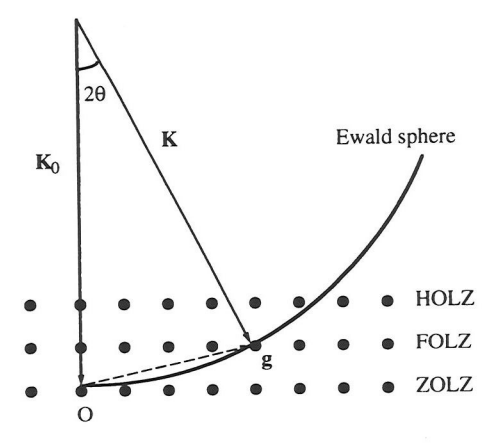


Figure 1.7. Construction of the Ewald sphere in reciprocal space, illustrating the electron-diffracting condition. Bragg reflections belonging to different Laue zones are indicated by dark spots.

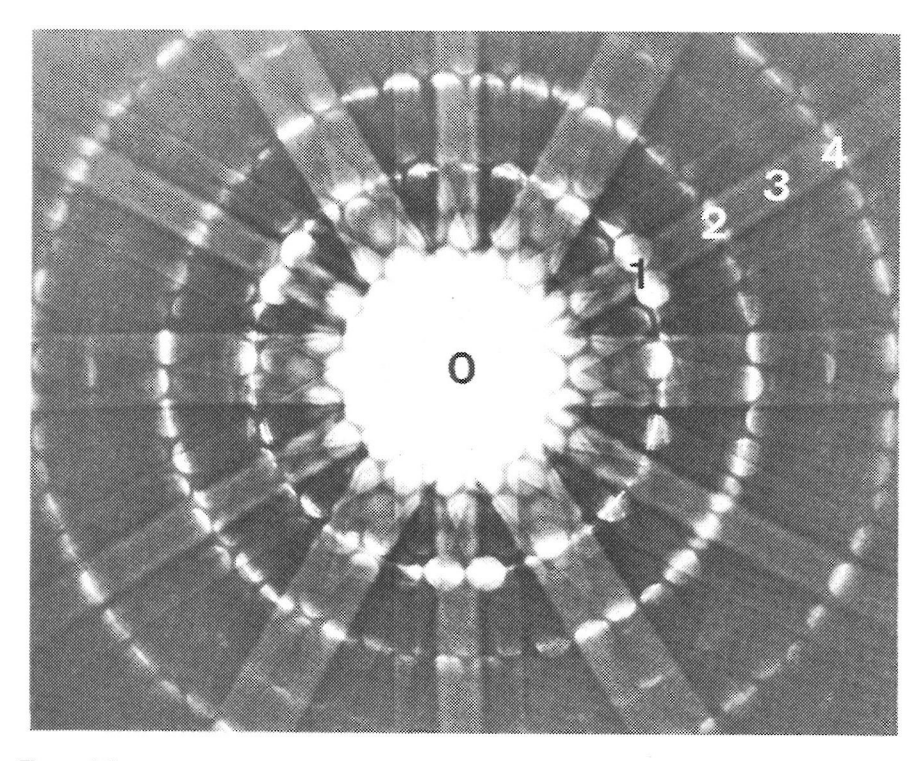


Figure 1.8. HOLZ reflections of an α -Al₂O₃ crystal viewed along [0001]. Numbers indicate corresponding orders of Laue circles. The diffraction pattern was recorded at 100 keV with a converged beam to enhance the intensity of the HOLZ rings.

in reciprocal space, as shown in Fig. 1.7. For elastic scattering, the conservation of energy requires $K = K_0 = 1/\lambda$; thus a sphere of radius K is drawn in reciprocal space with the wave vector of the incident electron beam ending at the origin. The wave vector of the diffracted beam is drawn from the center of the sphere, and the diffracted intensity at \mathbf{u} is $|V(\mathbf{u})|^2$. The possible beams generated in diffraction pattern are the reciprocal lattice vectors intersecting the Ewald sphere. Circles made by intersections of the Ewald sphere with the planes of reciprocal lattice vectors are called the Laue circles. The reflections are thus classified as the zero-order Laue zone (ZOLZ), the first-order Laue zone (FOLZ), and higher order Laue zones (HOLZs). The ZOLZ is usually defined as the plane of reciprocal lattice points that passes through the origin. An HOLZ is any other reciprocal lattice plane parallel to the plane of the ZOLZ, not passing through the origin, as illustrated in Fig. 1.7. The Ewald sphere construction is a simple and direct method for illustrating the diffracting conditions of electron diffraction. As demonstrated later, classifying

Bragg beams as ZOLZ and HOLZ reflections makes theoretical treatment very different.

Figure 1.8 shows an experimental diffraction pattern of [0001] α -Al₂O₃. The HOLZs are visible up to the fourth order. If the beam direction is parallel to c^* , the radius of the *m*th Laue zone ring is $u_m = (2c^*mK_0)^{1/2}$. Thus

$$u_{m+1}^2 - u_m^2 = 2c^* K_0$$

which can be used to measure the reciprocal lattice vector c^* . Besides HOLZs, Kikuchi bands are also observed. These are the results of electron inelastic scattering, and they are discussed in Part II of this book.

We now return to diffracting conditions. From Eq. (1.22), the projections of **u** on real space axes are

$$\mathbf{u} \cdot \mathbf{a} = \ell \quad \mathbf{u} \cdot \mathbf{b} = m \quad \mathbf{u} \cdot \mathbf{c} = n \tag{1.23}$$

which represent the well-known Laue conditions for diffraction. In reciprocal space, each reciprocal-space lattice point (ℓ, m, n) represents a set of equally spaced, parallel atomic planes in real space. When one plane is drawn through an atom in the unit-cell origin, the intercepts of the next parallel plane of the set on the axes are a/ℓ , b/m, and c/n. For an orthogonal unit-cell system, as shown in Fig. 1.9, the perpendicular distance between the adjacent planes of the set is

$$\frac{1}{d_g^2} = \frac{\ell^2}{a^2} + \frac{m^2}{b^2} + \frac{n^2}{c^2} \tag{1.24}$$

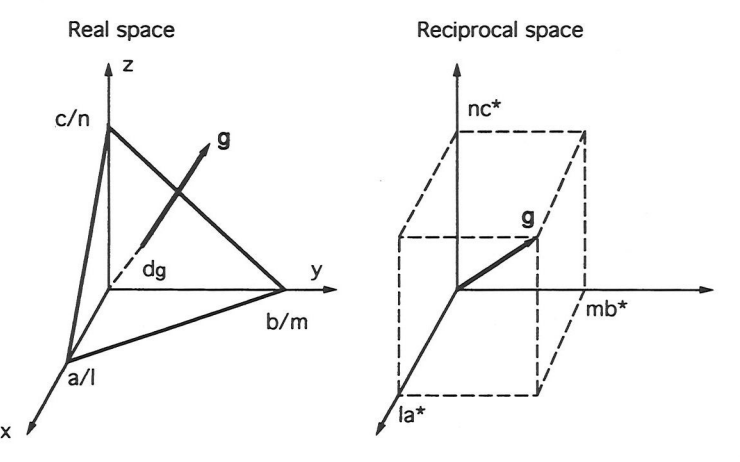


Figure 1.9. Relationships between (a) real-space atomic planes and the corresponding (b) reciprocal-space lattice vectors for an orthogonal crystal structure.

On the other hand, the distance from the reciprocal lattice origin to the (ℓ, m, n) reciprocal lattice point is the inverse of the distance between the adjacent atomic planes,

$$g = \frac{1}{d_g} \tag{1.25a}$$

and the vector perpendicular to the (\mathcal{C}, m, n) lattice planes is the vector from the origin to the (\mathcal{C}, m, n) reciprocal lattice point in reciprocal space. These relationships hold also for nonorthogonal axes. Using Eq. (1.25), the modulus of Eq. (1.22) is $u = 1/d_g$. Using the scattering angle defined in Fig. 1.2, Bragg's law is explicitly written as

$$2 d_g \sin \theta_g = \lambda \tag{1.25b}$$

This condition is similar to the $2d_g \sin \theta_g = \lambda$ law for light reflection from a semi-infinity medium. Thus the well-defined diffracted beam given by Eq. (1.25b) is conveniently referred to as the Bragg reflection. Equation (1.25b) is usually called the Bragg condition, under which the corresponding reciprocal lattice point intersects the Ewald sphere with zero excitation error.

The diffraction of electrons is classified as a Bragg case or a Laue case. In the Bragg case, an incident beam is diffracted from planes parallel or nearly parallel to the flat surface of a crystal that may be considered semi-infinite. Thus diffracted beams observed are those that reenter the vacuum on the same side of the crystal as the incident beam (Fig. 1.10a). Reflection high-energy electron diffraction

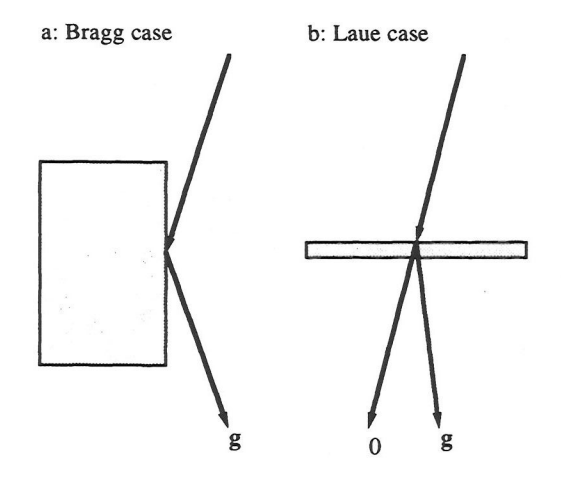


Figure 1.10. Diagrams showing the diffraction of electrons in the (a) Bragg and (b) Laue cases.

Basic Kinematic Electron Diffraction

(RHEED) from a bulk crystal surface and low-energy electron diffraction (LEED) are typical examples of Bragg cases. Hence the Bragg case is basically the case of backscattering. The dynamical diffraction of reflected electrons in RHEED is described in Chapter 5.

The Laue case involves transmission diffraction (without backscattering) through a parallel-sided crystal plate of infinite extent in two dimensions (Fig. 1.10b). This is the situation in TEM. Most of the following chapters discuss electron diffraction in the Laue case.

1.8. ABBE'S IMAGING THEORY

In TEM micrographs, image contrast is the result of electron scattering by atoms in the specimen and transfer properties of the optic system. The image formation is usually described by Abbe's theory, which is schematically shown in Fig. 1.11. The specimen is illuminated by a plane wave. The transmitted wave function $\Psi(x, y)$ at the exit face of the specimen can be assumed to be composed

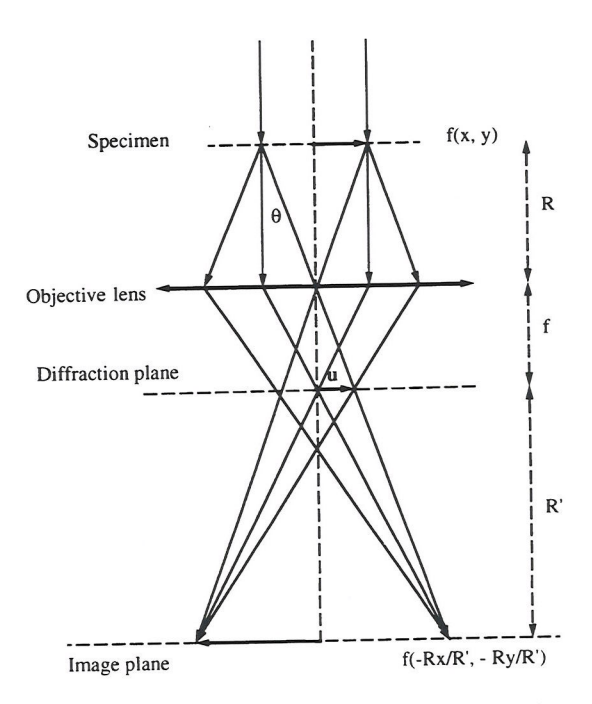


Figure 1.11. Abbe's theory of image formation in a TEM.

of a forward-scattered, axial, transmitted wave and other scattered waves that proceed in directions slightly inclined to it.

An ideal thin lens brings the parallel transmitted waves to a focus on the axis in the back focal plane. Waves leaving the specimen in the same direction (or angle θ with the optic axis) are brought together at a point on the back focal plane (or diffraction plane) at a distance $X = f \tan \theta$ from the axis, where f is the focal length. Thus on the back focal plane, waves from all parts of the illuminated regions propagating in a given direction are added. This is equivalent to the case in which the observation point is at infinity. So in the back focal plane, a Fraunhofer diffraction pattern is formed. The variable used for the distribution of the diffracted amplitude in the diffraction pattern for the one-dimension case is $u = 2K \sin(\theta) \approx 2\theta/\lambda$. Mathematically the formation of the Fraunhofer diffraction pattern is described by a Fourier transform (Cowley, 1981),

$$\Psi(\mathbf{u}) = \mathbf{FT} \left[\Psi(x, y, d) \right] \tag{1.26}$$

The formation of an image is then described by the inverse Fourier transform of the diffracting amplitude $\Psi(\mathbf{u})$

$$\Psi_i(x, y, d) = \mathbf{F} \mathbf{T}^{-1} [\Psi(\mathbf{u})] = \Psi(-x/M, -y/M, d)$$
 (1.27)

where the minus sign means the inversion of the object by the objective lens and M is the magnification of the lens. Equation (1.27) is for the case of an ideal objective lens. In general, the chromatic and spherical aberrations of the lens, as well as the size of the objective aperture, introduce a transfer function $T_{\rm obj}(\mathbf{u})$ for the optic system,

$$T_{\text{obj}}(\mathbf{u}) = A_{\text{obj}}(\mathbf{u}) \exp\left(\frac{1}{2}\pi i C_s \lambda^3 u^4 + \pi i \Delta f \lambda u^2\right)$$
(1.28a)

where A_{obj} is the shape function of the objective aperture, C_s is the spherical aberration coefficient of the lens, and Δf is the defocus of the lens. Thus Eq. (1.27) is modified as

$$\Psi_{i}(x, y, d) = \mathbf{F}\mathbf{T}^{-1}[\Psi(\mathbf{u}) \ T_{\text{obj}}(\mathbf{u})]$$

$$= \Psi(\mathbf{r}) \otimes \mathbf{F}\mathbf{T}^{-1}[T_{\text{obj}}(\mathbf{u})] = \int d\mathbf{b}' \ \Psi(\mathbf{b}', d) \ T_{\text{obj}}(\mathbf{b} - \mathbf{b}')]$$
(1.28b)

The diffraction pattern is given by

$$|\Psi(\mathbf{u})|^2 = |\mathbf{FT}[\Psi_i(x, y)]|^2 = |\int d\mathbf{b} \exp(-2\pi i \mathbf{u} \cdot \mathbf{b}) \Psi_i(\mathbf{b}, d)|^2$$
 (1.28c)

As a summary, Abbe's imaging theory is a two-step process—taking a Fourier transform of the electron wave function at the exit face of the crystal, then multiplying the lens transfer function and inversely Fourier-transforming the

diffraction amplitude back into real space. The electron diffraction pattern is a modulus square of the Fourier transformed wave function at the exit face of the crystal. Applications of Abbe's theory to approaching different imaging techniques are described in Chapters 11-13.

1.9. SOME MATHEMATICAL OPERATIONS

Several mathematical operations have been introduced, and they are frequently used in diffraction and imaging theories. This section outlines some basic features of these mathematical operations.

1.9.1. Fourier Transformation

The Fourier transform is mostly used to correlate electron waves in reciprocal space (or the diffraction plane) with those in real space (or the image plane), which is defined as

$$\Psi(\mathbf{u}) = \mathbf{FT}[\Psi(\mathbf{b})] = \int d\mathbf{b} \exp(-2\pi i \mathbf{u} \cdot \mathbf{b}) \ \Psi(\mathbf{b})$$
 (1.29a)

and the inverse Fourier transform is

$$\Psi(\mathbf{b}) = \mathbf{F}\mathbf{T}^{-1}[\Psi(\mathbf{u})] = \int d\mathbf{u} \exp(2\pi i \mathbf{u} \cdot \mathbf{b}) \ \Psi(\mathbf{u})$$
 (1.29b)

In this book, integral limits are $(-\infty, \infty)$ unless otherwise specified. The $(-\infty, \infty)$ integral limits are usually omitted in a mathematical expression for simplification.

The Fourier transformation is an important mathematical calculation in describing imaging and diffraction theories (Cowley, 1981). A useful relation in imaging theory is the Fourier transform of a plane wave

$$\delta(\mathbf{u} - \mathbf{K}_b) = \int d\mathbf{b} \exp(-2\pi i \mathbf{u} \cdot \mathbf{b}) \exp(2\pi i \mathbf{K}_b \cdot \mathbf{b})$$

It is important to point out that the Fourier transform of a function is denoted by the same symbol in this book, but the variable is replaced by u. The Fourier transform of $\Psi(\mathbf{b})$, for example, is denoted by $\Psi(\mathbf{u})$. It is also necessary to indicate that the sign of the phase factor in the Fourier transform is consistent in the entire book. Appendix B gives the general properties of the Fourier transform.

1.9.2. Convolution Calculation

A convolution calculation, denoted by \otimes , is usually applied in imaging theory, and it is defined by

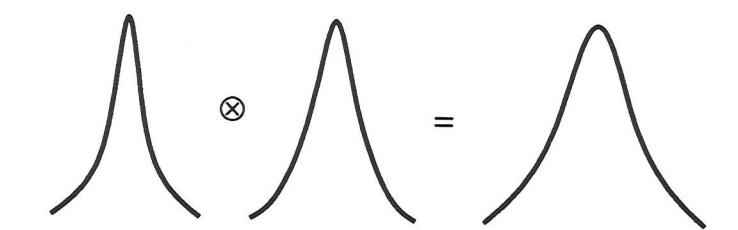


Figure 1.12. A schematic diagram showing the convolution result of two real functions.

$$F(\mathbf{b}) \otimes G(\mathbf{b}) = \int d\mathbf{b}' F(\mathbf{b} - \mathbf{b}') G(\mathbf{b}') = \int d\mathbf{b}' F(\mathbf{b}') G(\mathbf{b} - \mathbf{b}')$$
 (1.30)

The convolution of two functions commutes,

Basic Kinematic Electron Diffraction

$$F(\mathbf{b}) \otimes G(\mathbf{b}) = G(\mathbf{b}) \otimes F(\mathbf{b})$$
 (1.31)

The effect of convolution is to broaden the distribution profile of one function by that of another. This feature can be illustrated by the convolution of two Gaussian functions

$$\exp\left(-\frac{x^2}{a^2}\right) \otimes \exp\left(-\frac{x^2}{b^2}\right) = \frac{\pi^{1/2}ab}{(a^2 + b^2)^{1/2}} \exp\left(-\frac{x^2}{a^2 + b^2}\right) \ a, b > 0$$

A numerical plot of this calculation is illustrated in Fig. 1.12. The convolution calculation is applied in inelastic-scattering theory to characterize the angular redistribution and broadening of electrons due to inelastic excitations.

In electron diffraction calculation, the convolution theorem in Eqs. (1.32a-b) is often used. The Fourier transform of a product of two functions is the convolution of their Fourier transforms

$$\mathbf{FT}[F(\mathbf{b})\ G(\mathbf{b})] = \mathbf{FT}[F(\mathbf{b})] \otimes \mathbf{FT}[T(\mathbf{b})] = F(\mathbf{u}) \otimes G(\mathbf{u}) \tag{1.32a}$$

or

$$\mathbf{F}\mathbf{T}^{-1}[F(\mathbf{u}) \otimes G(\mathbf{u})] = F(\mathbf{b}) G(\mathbf{b}) \tag{1.32b}$$

This relation simply means that the convolution of two functions in reciprocal space is the result of a Fourier transform of the product of the two functions in real space. Equation (1.32b) can easily be proved using the variable substitution method

$$\mathbf{F}\mathbf{T}^{-1}[F(\mathbf{u}) \otimes G(\mathbf{u})] = \int d\mathbf{u} \exp(2\pi i \mathbf{u} \cdot \mathbf{b}) \int d\mathbf{u}' F(\mathbf{u} - \mathbf{u}') G(\mathbf{u}')$$
$$= \int d\mathbf{u} \int d\mathbf{u}' \exp[2\pi i (\mathbf{u} - \mathbf{u}') \cdot \mathbf{b}] F(\mathbf{u} - \mathbf{u}') \exp(2\pi i \mathbf{u}' \cdot \mathbf{b}) G(\mathbf{u}')$$

$$= \int d\mathbf{u}'' \exp[2\pi i \mathbf{u}'' \cdot \mathbf{b}] F(\mathbf{u}'') \int d\mathbf{u}' \exp(2'\pi \mathbf{u}' \cdot \mathbf{b}) G(\mathbf{u}')$$
$$= F(\mathbf{b}) G(\mathbf{b})$$

The convolution theorem is normally used in the multislice theory (Chapter 3) to convert the electron wave from real space to reciprocal space, and vise versa.

1.9.3. Dirac Delta Function

The δ function defined in Eqs. (1.33a-b) is frequently used in diffraction theory. For the two-dimensional case,

$$\delta(\mathbf{b}) = \begin{cases} 0 & \mathbf{b} \neq 0 \\ \infty & \mathbf{b} = 0 \end{cases}$$
 (1.33a)

and

$$\int d\mathbf{b} \,\delta(\mathbf{b}) = 1 \tag{1.33b}$$

The delta function can be considered the limit of a set of real continuous functions, such as gaussians

$$\delta(x) = \lim_{\chi \to 0} \left\{ \frac{1}{\pi \chi} \exp\left(-\frac{x^2}{\chi^2}\right) \right\}$$
 (1.34)

An important definition of the delta function, as applied to scattering, is

$$\delta(\mathbf{u} - \mathbf{u}') = \int d\mathbf{b} \exp[2\pi i (\mathbf{u} - \mathbf{u}') \cdot \mathbf{b}]$$
 (1.35)

A very useful relation for converting a summation over unit cells in real space into a summation of reciprocal lattice vectors is

$$\sum_{n=-\infty}^{\infty} \exp(2\pi i \mathbf{R}_n \cdot \mathbf{u}) = \sum_{g} \delta(\mathbf{u} - \mathbf{g})$$
 (1.36)

The basic features of the delta function are given in Appendix C. The delta function has two important properties:

The delta function is a symmetric function

$$\delta(\mathbf{b}) = \delta(-\mathbf{b}) \tag{1.37a}$$

The convolution of the delta function with a continuous function is the function itself

$$\int d\mathbf{b}' F(\mathbf{b}') \, \delta(\mathbf{b} - \mathbf{b}') = F(\mathbf{b}) \otimes \delta(\mathbf{b}) = F(\mathbf{b}) \tag{1.37b}$$

Applications of these properties are illustrated in subsequent chapters.

Basic Kinematic Electron Diffraction

Kinematical scattering theory, as the base of analyzing electron diffraction patterns, is important for understanding the dynamical scattering theory. In Chapter 1, based on the first Born approximation, the electron scattering factor, reciprocal space and reciprocal lattice vectors are introduced. The Ewald sphere is a simple, elegant geometrical interpretation of electron diffraction. Many of the imaging and diffraction techniques to be introduced in Chapter 2 can be understood from the Ewald sphere construction. Fourier transform, convolution calculation and delta function are very useful mathematical tools for describing electron diffraction. Chapter 1 is a preliminary chapter that is indispensable for describing the dynamical theories in the remaining chapters of this book.